Acoustic microscopy of functionally graded thermal sprayed coatings using stiffness matrix method and Stroh formalism

Xiaodong Deng, Thomas Monnier, Philippe Guy, Joel Courbon

Acoustic microscopy of functionally graded thermal sprayed coatings using stiffness matrix method and Stroh formalism

X. D. Deng[1], T. Monnier[2,a)], P. Guy[2] and J. Courbon[1]
[1]Université de Lyon, INSA-Lyon, MATEIS UMR5510, F-69621 Villeurbanne, France
[2]Université de Lyon, INSA-Lyon, LVA EA 677, F-69621 Villeurbanne, France

[a)] Corresponding author:
Associate professor T. Monnier
Université de Lyon, INSA-Lyon, LVA EA 677,
F-69621 Villeurbanne cedex, France
Tel: +33 (0) 4 72 43 62 99
Fax: +33 (0) 4 72 43 88 22
E-mail address: thomas.monnier@insa-lyon.fr

Abstract

Acoustic microscopy of multilayered media as well as functionally graded coatings on substrate necessitates to model acoustic wave propagation in such materials. In particular, we chose to use Stroh formalism and the recursive stiffness matrix method to obtain the reflection coefficient of acoustic waves on these systems because this allows us to address the numerical instability of the conventional transfer matrix method. In addition, remarkable simplification and computational efficiency are obtained. We proposed a modified formulation of the angular spectrum of the transducer based on the theoretical analysis of a line-focus transducer for broadband acoustic microscopy. A thermally sprayed coating on substrate is treated as a functionally graded material along the depth of the coating and is approximately represented by a number of homogeneous elastic layers with exponentially graded elastic properties. The agreement between our experimental and numerical analyses on such thermal sprayed coatings with different thickness confirms the efficiency of the method. We proved the ability of the inversion procedure to independently determine both thickness and gradient of elastic properties. The perspective of this work is the opportunity to non-destructively measure these features in functionally graded materials.

I. INTRODUCTION

Acoustic microscopy, as first proposed by Quate *et al.*[1,2], and further developed by Briggs *et al.*[3], has been used as a useful nondestructive technique to characterize the elastic properties of layered structures and to inspect the quality of bound between layer and substrate[3,4]. This technique is based on

the measurement of the acoustic signature or the material, also named *V(z)* curve, which refers to the variation of the normalized output voltage of an ultrasonic sensor as a function of the separation distance *z* between the focal point of the acoustic lens and the plane surface of a reflecting object. This curve is characteristic of the sample material, with the spacing of the dips over the negative part of the *z* range relating to the magnitude of the surface wave speed.[5,6]

Several methods have been developed in order to analyze the acoustic response of focused transducers, i.e. the *V(z)* curve, either for isotropic or anisotropic homogeneous materials as well as for layered or coated systems. In harmonic situation, method such as paraxial approximation[6,7] and non-paraxial angular spectrum[8] approaches can be applied. The angular-spectrum approach along with the paraxial approximation was proposed to derive the expression of *V(z)* curve in terms of the reflection function by Atalar.[6] This method was then developed to analyze a line-focus system in microscopy by *Li et al.*[7] This angular-spectrum approach was widely used to study *V(z)* curves of films and/or coatings and layered anisotropic materials and can be employed to measure elastic constants of thin-films and to detect of surface cracks in materials and components.[9-11] Other methods, such as ray-optics[12] or Fourier optics[13], asymptotic approach[14] and modified ray approach[15] can also be used to model *V(z)* curves. For spherical transducers, an expression of *V(z)* in the frequency domain for a large-aperture broadband transducer was derived by Zhang.[16] In the field of numerical analysis, a combined finite element method/boundary element method was used for *V(z)* analysis of inhomogeneous layers by Liu.[17] Despite all these progresses in acoustic microscopy, the study of *V(z)* curves of coatings with graded physical and/or elastic properties deposited on substrate misses a few developments.

Apart from the diffraction phenomena due to geometry of the transducer, one of the most important quantity to be determined in the calculation of *V(z)* curve is the global reflection coefficient $R(\theta,f)$ of acoustic waves onto the multilayered system. $R(\theta,f)$ is a function of the incident angle (θ) and the frequency (f). Many methods, such as transfer matrix method[18-23], delta matrix method[24], invariant embedding method or scattering-matrix method,[25,26] and stiffness matrix method[27,28] have been developed for the calculation of acoustic reflection coefficients as well as the analysis of surface acoustic waves on a multilayered elastic isotropic and/or anisotropic media. A remarkable review of these methods can be found in the thesis of C. Baron[29]. However, it is recognized that the transfer matrix method becomes computationally instable for high frequency-thickness products ($f\times d$).[11,20,25,27] The delta matrix method was proposed to overcome the problems of numerical instability, but the need to introduce complicate delta matrix operators makes this method difficult to apply.[24] The invariant embedding method and scattering-matrix method deal with reflection and transmission matrices for individual interfaces and then recursively combines them into global reflection and transmission matrices for a layered system, and they are numerically stable. Another way of dealing with the instability of the transfer matrix method is to develop a stiffness matrix method as proposed by Wang and Rokhlin.[27,28] This method reformulates the transfer matrix in the form of a stiffness matrix, which relates displacements to stresses on both sides of each layer. By virtue of the computational stability and efficiency of the stiffness matrix method for any anisotropic multilayered medium, we used it as the basis of the hybrid transform method developed in the present paper. We adopted the Stroh formalism for the calculation of the reflection coefficient and the modeling of *V(z)* curve on systems consisting of thermal coatings sprayed on metallic substrates.

In the present article, a theoretical analysis of the *V(z)* curve obtained with of a broadband a relatively low-frequency line-focus (or cylindrical) transducer is proposed. The reflection coefficient formula for coatings with graded properties, deposited on metallic substrate and immerged in fluid is derived based on Stroh formalism. Both theoretical and experimental results are presented and discussed.

II. THEORETICAL MODEL

A. Method and hypotheses

The general setup of a line-focus transducer sketched in Fig. 1a, represents a cut perpendicular to the generatrix of the cylindrical transducer, which is machined to form a line-focus. We suppose that all the points of the radiating surface vibrate in phase and have uniform amplitude of particle velocity. The half aperture β has to be large enough to be able to excite leaky Rayleigh waves in most solids. The distance between the water-specimen interface and the focal plane is denoted z. By convention, the focal position corresponds to z=0, and the displacement of the specimen away from the transducer is taken as positive. We assume that the specimen is a solid plane reflector and also assume that the coupling fluid (pure water) is ideal. Finally, the radiation of the acoustic waves will be expressed by using the angular spectrum approach.[11]

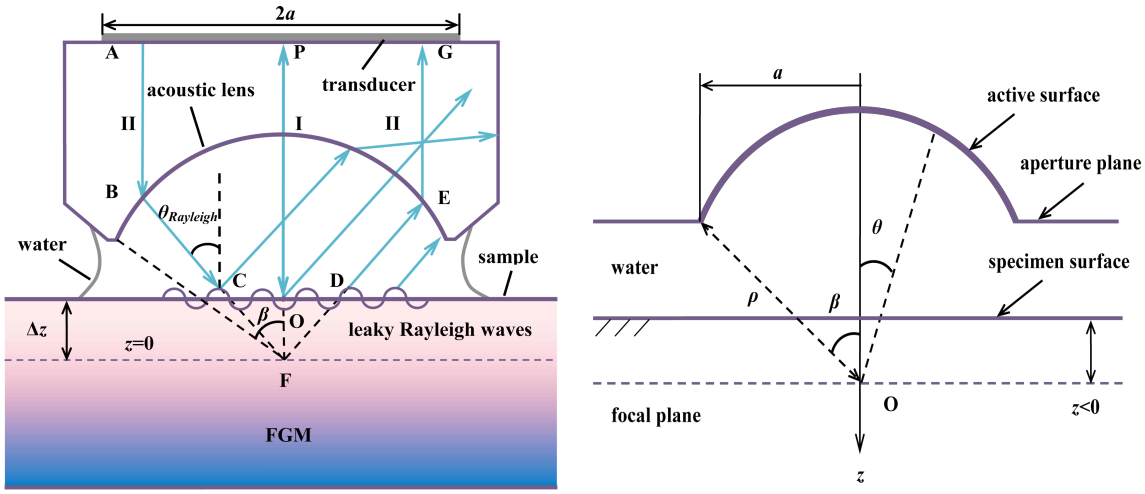

(a) (b)

FIG. 1. Sketch of line-focus acoustic microscopy on (a) a functionally graded material and (b) a set-up of the experiment.

This formulation is valid for plane waves and is applicable for a wide aperture angle transducer relying on the fact the secondary diffraction due to the curvature of the wavefront can be ignored when the size of the source is large in comparison to the wavelength, and when the transducer works in pulse-echo mode.[16] The short wavelength requirement is easily satisfied since the interest is not put on very low frequencies for which efficient focusing cannot be realized.

B. Angular spectrum approach and *V(z)* integral

Based on the work of Lee *et al.*,[11] the output voltage of the line-focus transducer can be written as:

$$V(z) = \int_{-\infty}^{+\infty} \exp(2ik_z z) L_1(k_x) L_2(k_x) R(k_x) dk_x, \quad (1)$$

where k_x and $k_z = \sqrt{k_f^2 - k_x^2}$ are the horizontal and vertical components of the wave vector respectively, k_f is the magnitude of the wave vector in the coupling fluid, $R(k_x)$ is the reflection coefficient of the fluid-loaded specimen, $L_1(k_x)$ is the angular spectrum of the incident wave field at the focal plane and $L_2(k_x)$ is the response of the transducer when a plane wave of unit amplitude and wave vector (k_x, k_z) is

insonifying the lens. The expressions of these characteristic functions of the acoustic lens can be found in Ref. 11 and are not transcribed here. Knowing that in our line-focus transducer, made of polyvinylidene fluoride (PVDF), is directly machined to form a line-focus transducer (Fig. 1b) the radius of curvature is also the focal distance of the transducer and the acoustic lens part is excluded. This leads L_1 to be equal to L_2, whose expression is given by:

$$L_1(k_x) = L_2(k_x) = i\rho\int_{-\beta}^{\beta} \exp\left(k_x \sin(\theta) + \sqrt{k_f^2 - k_x^2}\cos(\theta)\right)d\theta, \tag{2}$$

where θ is the incident angle on the specimen and β is the half aperture of the transducer.

C. Derivation of the reflection coefficient for a multilayered system

For a multilayered (N-layer) system bounded onto a substrate, we assume an ultrasonic incident wave in a fluid as shown in Fig. 2.

In the Stroh formalism[31], the governing equation for the state vector $\boldsymbol{\xi} = \begin{bmatrix} \mathbf{U} \\ \mathbf{T} \end{bmatrix}$, where and $\boldsymbol{U}$ is the general displacement vector and $\boldsymbol{T}$ is the general stress on the x-y plane, is represented by a system of differential equations:

$$\frac{d\boldsymbol{\xi}}{dz} = i\mathbf{A}(z)\boldsymbol{\xi}. \tag{3}$$

For purely elastic problems, $\mathbf{U} = \left[u_x, u_y, u_z\right]^T$ and $\mathbf{T} = \left[\sigma_{xz}, \sigma_{yz}, \sigma_{zz}\right]^T$ are the particle displacements and normal stress vectors respectively.

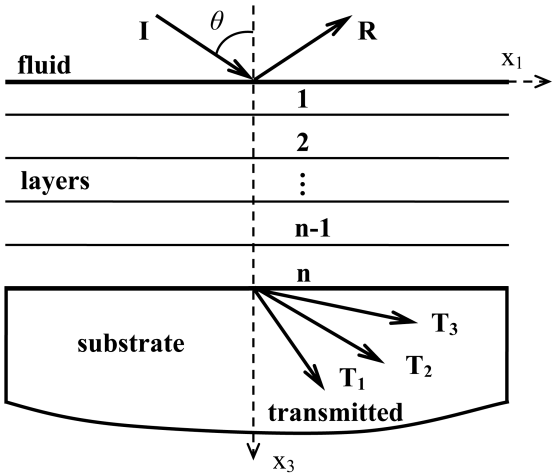

FIG. 2. Sketch of fluid loaded multi-layered coatings on substrate.

Considering a harmonic wave propagating along the x-axis of the form $\xi(z)e^{i(\omega t - k_x x)}$, then the governing Eq. (3) can be written as a linear system of equations in terms of the state vector.[32-35] Then $\boldsymbol{A}$ is the fundamental acoustic tensor, which can be written as a (6×6) matrix whose terms are related to the elastic properties of the material[19,36].

To solve Eq. (3), Wang[36] introduced the state transfer matrix $\boldsymbol{B}$ to relate the state vector $\xi(z)$ at z to the state vector $\xi(z_0)$ at z_0 according to:

$$\boldsymbol{\xi}(z) = \mathbf{B}(z, z_0)\boldsymbol{\xi}(z_0). \tag{4}$$

Substituting Eq. (4) into Eq. (3), the relationship between matrices $\boldsymbol{B}$ and $\boldsymbol{A}$ can be obtained

$$\frac{d\mathbf{B}(z, z_0)}{dz} = i\mathbf{A}(z)\mathbf{B}(z, z_0), \quad \mathbf{B}(z_0, z_0) = \mathbf{I}. \tag{5}$$

For homogeneous layer between z_0 and z_1, $\boldsymbol{A}$ is a constant matrix. Then, the transfer matrix $\boldsymbol{B}$ can be written in the form of a matrix exponential:

$$\mathbf{B}(z_1, z_0) = e^{i\mathbf{A}h}, \tag{6}$$

where $h = z_1$-z_0, is the thickness of the layer.

For a multilayer medium, the transfer matrix of the nth layer satisfies:

$$\begin{bmatrix} \mathbf{U}(z_n) \\ \mathbf{T}(z_n) \end{bmatrix} = \mathbf{B}(n) \begin{bmatrix} \mathbf{U}(z_{n-1}) \\ \mathbf{T}(z_{n-1}) \end{bmatrix}. \tag{7}$$

The total transfer matrix B relates the state vector at the bottom to the one at the top surface of the layered coating as follows:

$$\begin{bmatrix} \mathbf{U}(z_n) \\ \mathbf{T}(z_n) \end{bmatrix} = \mathbf{B}_{coat} \begin{bmatrix} \mathbf{U}(z_0) \\ \mathbf{T}(z_0) \end{bmatrix}. \tag{8}$$

Hence, $\boldsymbol{B}_{total}$ is expressed by the product of the transfer matrix $\boldsymbol{B}_n$ of each layer as:

$$\mathbf{B}_{\text{coat}} = \prod_{i=1}^{n} \mathbf{B}(i). \tag{9}$$

It is worth mentioning that as the layer thickness increase, the transfer matrix $\boldsymbol{B(n)}$ in Eq. (7) becomes numerically instable. To address this issue, Wang and Rokhlin[27] proposed the Reverse Stiffness Matrix method. First, the transfer matrix $\boldsymbol{B(n)}$ of the nth layer is transformed into a stiffness matrix as:

$$\mathbf{K}_n = \begin{bmatrix} -(\mathbf{B}_n^{12})^{-1}\mathbf{B}_n^{11} & (\mathbf{B}_n^{12})^{-1} \\ \mathbf{B}_n^{21} - \mathbf{B}_n^{22}(\mathbf{B}_n^{12})^{-1}\mathbf{B}_n^{11} & \mathbf{B}_n^{22}(\mathbf{B}_n^{12})^{-1} \end{bmatrix}, \tag{10}$$

where $\mathbf{B}_n^{ij}$ $(i,j=1,2)$ are the 3×3 submatrices of the transfer matrix of the nth layer $\boldsymbol{B(n)}$. Then, the total stiffness matrix from the bottom to the top of the layer is obtained by using a recursive algorithm as:

$$\mathbf{K}^M = \begin{bmatrix} \mathbf{K}_{11}^{M-1} + \mathbf{K}_{12}^{M-1}(\mathbf{K}_{11}^{m} - \mathbf{K}_{22}^{M-1})^{-1}\mathbf{K}_{21}^{M-1} & -\mathbf{K}_{12}^{M-1}(\mathbf{K}_{11}^{m} - \mathbf{K}_{22}^{M-1})^{-1}\mathbf{K}_{12}^{m}) \\ \mathbf{K}_{21}^{m}(\mathbf{K}_{11}^{m} - \mathbf{K}_{22}^{M-1})^{-1}\mathbf{K}_{21}^{M-1} & \mathbf{K}_{22}^{m} - \mathbf{K}_{21}^{m}(\mathbf{K}_{11}^{m} - \mathbf{K}_{22}^{M-1})^{-1}\mathbf{K}_{12}^{m} \end{bmatrix}, \tag{11}$$

where $\boldsymbol{K}^M$ is the total stiffness matrix for the top m layers, $\boldsymbol{K}^{M-1}$ is the total stiffness matrix for the top m-1 layers, $\boldsymbol{K}^m$ are stiffness matrix elements for the mth layer. Finally the expression of the total transfer matrix in Eq. (9) is:

$$\mathbf{B}_{coat} = \begin{bmatrix} -(\mathbf{K}_M^{12})^{-1}\mathbf{K}_M^{11} & (\mathbf{K}_M^{12})^{-1} \\ (\mathbf{K}_M^{21}) - \mathbf{K}_M^{22}(\mathbf{K}_M^{12})^{-1}\mathbf{K}_M^{11} & \mathbf{K}_M^{22}(\mathbf{K}_M^{12})^{-1} \end{bmatrix}, \tag{12}$$

where K_M^{ij} $(i,j=1,2)$ are the 3×3 submatrices of the total stiffness matrix $\boldsymbol{K}^M$.

For the substrate, we choose to use the matrix decomposition method employed by Wang and Rokhlin[36]. First, the transfer matrix of substrate $\boldsymbol{B}_{sub}$ is calculated by Eq. (6), and decomposed in the following form:

$$\mathbf{A}_{sub} = \begin{bmatrix} \mathbf{P}^- & \mathbf{P}^+ \\ \mathbf{D}^- & \mathbf{D}^+ \end{bmatrix} \begin{bmatrix} \mathbf{H}^- & \mathbf{0} \\ \mathbf{0} & (\mathbf{H}^+)^{-1} \end{bmatrix} \begin{bmatrix} \mathbf{P}^- & \mathbf{P}^+ \\ \mathbf{D}^- & \mathbf{D}^+ \end{bmatrix}^{-1}, \tag{13}$$

where the "–" and "+" superscripts represent the wave propagation in the –z and +z direction respectively, $\mathbf{P}^{\pm}$ and $\mathbf{D}^{\pm}$ represent the displacement polarization vector of the plane waves and the corresponding amplitude of stress components in the *x*-*y* plane respectively, and $\mathbf{H}^{\pm}$ is a diagonal matrix with the main diagonal containing the six eigenvalues of k_z in its exponential form. It was observed that this matrix decomposition method gives the same result than methods that traditionally solve the Christoffel equation and aim at obtaining the wavenumbers k_z.[27,37]

For a substrate with a semi-infinite depth, we assume that there is no reflection from the bottom of the substrate. Thus, the state vector at the top surface of the substrate can be rearranged as:

$$\begin{bmatrix} \mathbf{U} \\ \mathbf{T} \end{bmatrix}_{sub} = \begin{bmatrix} \mathbf{P}^- & \mathbf{P}^+\mathbf{H}^+ \\ \mathbf{D}^- & \mathbf{D}^-\mathbf{H}^+ \end{bmatrix}_{sub} \begin{bmatrix} \mathbf{A}_m^- \\ \mathbf{0} \end{bmatrix} \tag{14}$$

with

$$\mathbf{A}_m^- = \left[T_1, T_2, T_3\right]^T, \tag{15}$$

where, T_1, T_2 and T_3 are the amplitudes of the longitudinal and the two transversal waves transmitted in the substrate (as illustrated in Fig. 2) respectively. Then, we obtain:

$$\begin{bmatrix} \mathbf{U}(z_0) \\ \mathbf{T}(z_0) \end{bmatrix} = \mathbf{B}_{coat}^{-1} \times \begin{bmatrix} \mathbf{P}^- \\ \mathbf{D}^- \end{bmatrix}_{sub} \times \begin{bmatrix} T_1 \\ T_2 \\ T_3 \end{bmatrix} \tag{16}$$

where, $\begin{bmatrix} \mathbf{U}(z_0) \\ \mathbf{T}(z_0) \end{bmatrix}$ is the state vector at the top surface of the coating.

Now, taking into consideration the boundary condition on the fluid/layer interface yields:

$$\begin{bmatrix} u_x^0 \\ u_y^0 \\ u_z^0 \\ \sigma_{xz}^0 \\ \sigma_{yz}^0 \\ \sigma_{zz}^0 \end{bmatrix} = \begin{bmatrix} 1 & 0 & 0 \\ 0 & 1 & 0 \\ 0 & 0 & \cos\theta / V_f \\ 0 & 0 & 0 \\ 0 & 0 & 0 \\ 0 & 0 & -i\omega\rho_f \end{bmatrix} \begin{bmatrix} u_x^0 \\ u_y^0 \\ R \end{bmatrix} + \begin{bmatrix} 0 \\ 0 \\ -\cos\theta / V_f \\ 0 \\ 0 \\ -i\omega\rho_f \end{bmatrix} A_{in} = \mathbf{M} \times \begin{bmatrix} T_1 \\ T_2 \\ T_3 \end{bmatrix} \tag{17}$$

where $\boldsymbol{R}$ is the reflection coefficient and $\boldsymbol{A_{in}}$ is the incident acoustic amplitude and the matrix $\boldsymbol{M}$ is defined by:

$$\mathbf{M} = \mathbf{B}_{total}^{-1} \times \begin{bmatrix} \mathbf{P}^- \\ \mathbf{D}^- \end{bmatrix}_{sub}. \tag{18}$$

Finally, by choosing the incident wave amplitude $\boldsymbol{A}_{in}$ as unity, the linear equation of Eq. (17) is solved using Cramer's rule, and the obtained reflection coefficient is:

$$\mathbf{R} = \frac{\mathbf{Z}_1 - Q\mathbf{Z}_2}{\mathbf{Z}_1 + Q\mathbf{Z}_2}, \tag{19}$$

with

$$\mathbf{Z}_1 = \begin{vmatrix} \mathbf{M}_{41} & \mathbf{M}_{42} & \mathbf{M}_{43} \\ \mathbf{M}_{51} & \mathbf{M}_{52} & \mathbf{M}_{53} \\ \mathbf{M}_{61} & \mathbf{M}_{62} & \mathbf{M}_{63} \end{vmatrix}, \quad \mathbf{Z}_2 = \begin{vmatrix} \mathbf{M}_{31} & \mathbf{M}_{32} & \mathbf{M}_{33} \\ \mathbf{M}_{41} & \mathbf{M}_{42} & \mathbf{M}_{43} \\ \mathbf{M}_{51} & \mathbf{M}_{52} & \mathbf{M}_{53} \end{vmatrix}, \quad Q = i\omega\rho_f V_f / \cos\theta .$$

where, $\boldsymbol{M}_{ij}$ is the *(i,j)* element of the matrix $\boldsymbol{M}$ in Eq. (18).

In the case of a substrate without coating, the matrix $\boldsymbol{M}$ in Eq. (18) is simplified as follows:

$$\mathbf{M} = \begin{bmatrix} \mathbf{P}^- \\ \mathbf{D}^- \end{bmatrix}_{sub}. \tag{20}$$

and the formula used to compute the reflection coefficient remains as defined by Eq. (19).

D Identification of propagation modes: dispersion curves

The reflection coefficient calculated by Eq. (19) can be used for parametric studies, and the phase velocities of the possible surface acoustic wave (SAW) modes and their corresponding mode reflection coefficients can be predicted for an arbitrary system of coating on substrate. Thus the Eq. (19) can be used as a predictive formula to estimate which frequency should be applied for the characterization of a certain kind of coated material. The vanishing of its denominator is the characteristic equation of the layered medium on substrate.

$$\mathbf{Z}_1 + Q\mathbf{Z}_2 = 0 \tag{21}$$

Numerically solving this equation gives the phase velocity and the amplitude of the possible wave modes. One can note that setting $Q = 0$ in Eq. (21) excludes the effects of the fluid loading and thus identifies the free wave modes.[30,37]

For a given frequency, the reflection coefficient is a function of the incident angle θ. When the incident angle θ passes a critical angle θ_{cr}, the reflection coefficient undergoes a -2π phase shift and its real part undergoes a jump, which identifies a wave mode. The phase velocity is calculated according to Snell's law at the critical angle:

$$c = \frac{c_f}{\sin\theta_{cr}}. \tag{22}$$

In order to carry out the parametrical study and to estimate the possible SAW wave modes, we calculated the reflection coefficient for different thicknesses of a 22-type Hastelloy coating on a 304-type austenitic stainless steel substrate at different frequencies using Eq. (19). The dispersion curve and the corresponding reflection coefficient are presented in Fig. 3.

Fig. 3(a) shows that surface acoustic wave (SAW) with identity reflection coefficient exists all over the $f \times d$ range. Its phase velocity firstly undergoes a small decrease from the Rayleigh wave velocity of the substrate, and then goes to the Rayleigh wave velocity of the layer. This kind of so-called true SAW wave, as named by Guo *et al.*[38], is strongly reflected and can be easily picked up by a line-focus microscopy at small $f \times d$. Pre-Rayleigh waves, also named by Guo *et al.*[38] may exist and their phase velocities decrease from a velocity lower than the longitudinal velocity of the layer V_L at small $f \times d$ to the Rayleigh wave velocity of the layer at high $f \times d$, which is slightly below the shear velocity of the layer V_S. Still higher wave modes propagate at velocities higher than the longitudinal velocity of the layer. These generalized Lamb wave modes appear after certain cut-off frequency thickness product with decreasing phase velocity except some small fluctuation and they have smaller reflection coefficients. The same authors[38] demonstrated that these kinds of waves could also be picked up by line-focus microscopy as their reflection coefficients reach a higher level. In this study, the operating frequency of the transducer is in the range of 0 to 20 MHz, with a coating layer thickness around 200 μm, which gives a $f \times d$ range of 0 to 4 MHz·mm. This guarantees that the transducer picks up the true SAW wave.

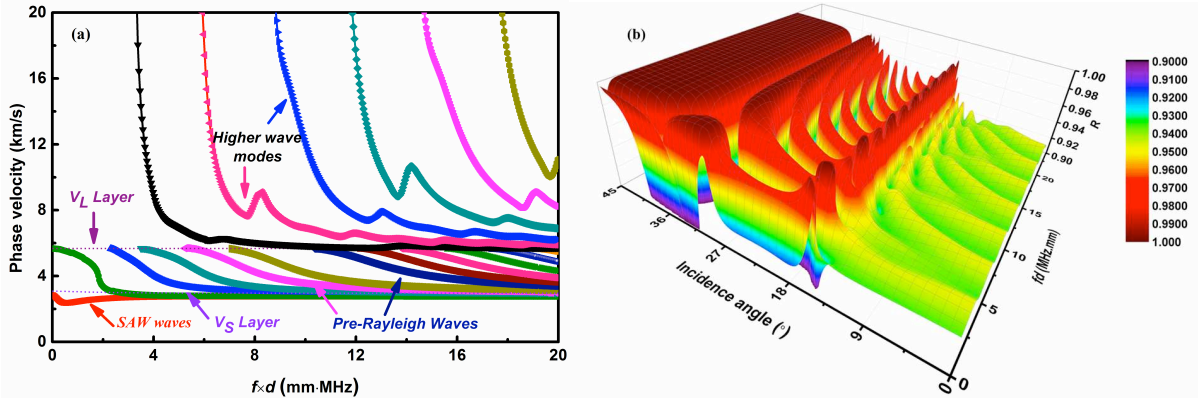

(a) (b)

FIG. 3. Dispersion curve of the 22-type Hastelloy coating on the substrate of 304-type austenitic stainless steel: (a) wave mode velocity and (b) 3D reflection coefficient.

III. EXPERIMENTAL SETUP

A schematic of our experimental setup is shown in Fig. 1b. The line-focus ultrasonic transducer was designed and constructed in our laboratory.[16] The piezoelectric element is a Polyvinylidene fluoride (PVDF) material, coated with a thin layer of gold. By a proper choice of the damping material for the backing, this transducer behaves as a broadband device. The radius of curvature of the transducer is 8 mm. The half-aperture angle is 36°, which is large enough for the generation of Rayleigh waves on most of the usual solids.

The transducer is connected to a commercially available pulse generator (33250A function/arbitrary waveform generator, Agilent Technologies, Inc.) by a preamplifier working in pulse-echo mode. In these conditions, it is possible to operate with transient signals whose frequency content extends from 5 to several tens of MHz. A digital oscilloscope (Tektronix TDS3012B), together with a personal computer, is used to record and process the time signals. The specimen is immerged in water whose temperature was well controlled by a thermal monitor with a constant temperature of 25 °.

During $V(z)$ curve measurement, both the specimen and the transducer are mounted on a mechanical translation stage (x, y, z, and rotation controllable) for accurate alignment and for the upward or

downward movement along the z axis. The transient response are obtained directly from the output of the system; while the $V(z)$ curves are obtained by fast Fourier transforming a series of transient responses measured at different distances z and then plotted as a function of z at a fixed frequency.

In this study, two kinds of materials are investigated. One is a bulk Inconel 600 stainless steel with finely measured properties such as density, longitudinal velocity and transversal velocities. This kind of material is used in order to validate $V(z)$ modeling of the line-focus microscopy, which will be discussed in Sec. IV.A. The other is a 22-type Hastelloy coating on a substrate of 304-type austenitic stainless steel. This material is chosen for the establishment and verification of the acoustic wave propagation model of a multilayered system on substrate, which will be presented in details in Sec. IV.B. The properties of the materials numerically investigated in this article are listed in Table I.

TABLE I. Properties of the materials used in this paper.

Testing Materials	ρ (g/cm^3)	E (GPa)	σ	V_L (m/s)	θ_L (°)†	V_S (m/s)	θ_S (°)†	V_R (m/s)	θ_R (°)†
Inconel 600	8.490	216.61	0.302	5878	14.68	3130	28.43	2899	30.93
304 steel	7.900	193.20	0.290	5661	15.26	3079	28.94	2846	31.57
22-type Hastelloy	8.690	199.00	0.314	5669	15.24	2952	30.31	2739	32.96

†Values calculated with sound velocity in water V_f= 1490 m/s.

IV. RESULTS AND DISCUSSION

A. *V(z)* curves of Inconel 600 bulk material

Fig. 4 is a comparison between experimental data and modeling on an Inconel 600 bulk material at 18.5 MHz. The $V(z)$ curve in red is calculated based on Eq. (19), and the dotted line in blue is measured using a line-focus transducer. To simplify the modeling, the reflection coefficient $\boldsymbol{R}$ in Eq. (19), i.e., the Inconel 600 bulk material immerged in coupling fluid (water) is calculated based on the canonical Brekhovskikh model, which can be expressed as[39]:

$$R = \frac{\left(Z_l \cos^2 2\theta_s + Z_s \sin^2 2\theta_s\right) - Z}{\left(Z_l \cos^2 2\theta_s + Z_s \sin^2 2\theta_s\right) + Z}, \tag{23}$$

where Z is the normal impedance of the fluid, Z_l the longitudinal normal impedance of the solid, Z_s the transversal normal impedance of the solid, and θ_s the transversal wave angle in the solid. It shows a reasonably good agreement with the measured $V(z)$ curve, what validates our model for a line-focus transducer. In Fig. 4 the modeling $V(z)$ curve is derived by an optimization process with changing parameters of the transducer, i.e., the radius of curvature of the transducer (ρ) and the half-aperture angle (β), with fixed parameters of the material and the applying frequency. The discrepancy between the

modeling and experiment may be due to the *V(z)* experimental error and measurement error of the Inconel 600 bulk material properties.

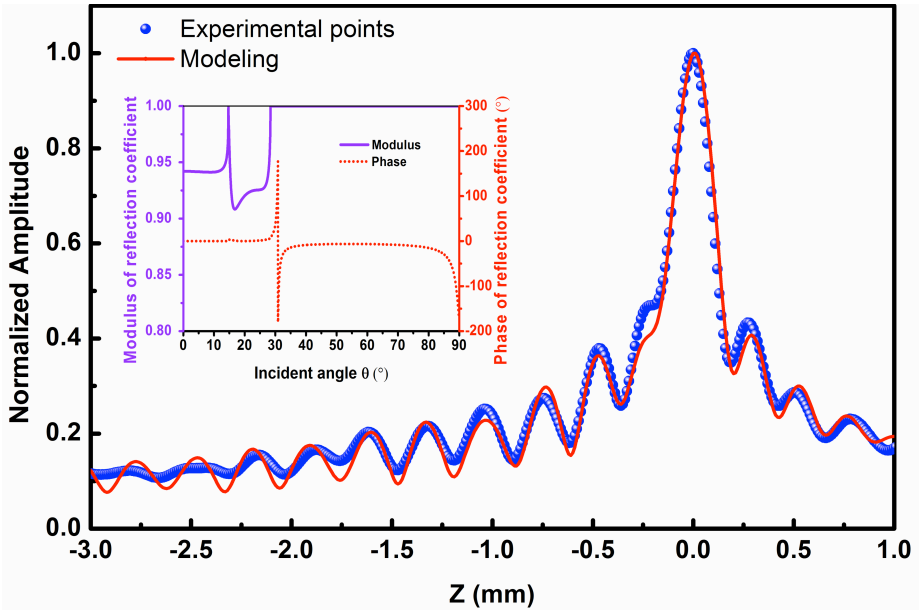

FIG. 4. Comparison between experiment and modeling of *V(z)* curves for an Inconel 600 bulk material at 18.5 MHz. Inset shows the reflection coefficient of the Inconel 600 bulk material immerged in water, whose temperature was well controlled by a thermal monitor with a constant temperature of 25 °.

In order to validate the formula for the reflection coefficient derived in Sec. II.C, comparison of the reflectance coefficient of Inconel 600 calculated based on Eq. (19) and the Brekhovskikh formula Eq. (23) is presented in Fig. 5. It shows an excellent agreement between these two models.

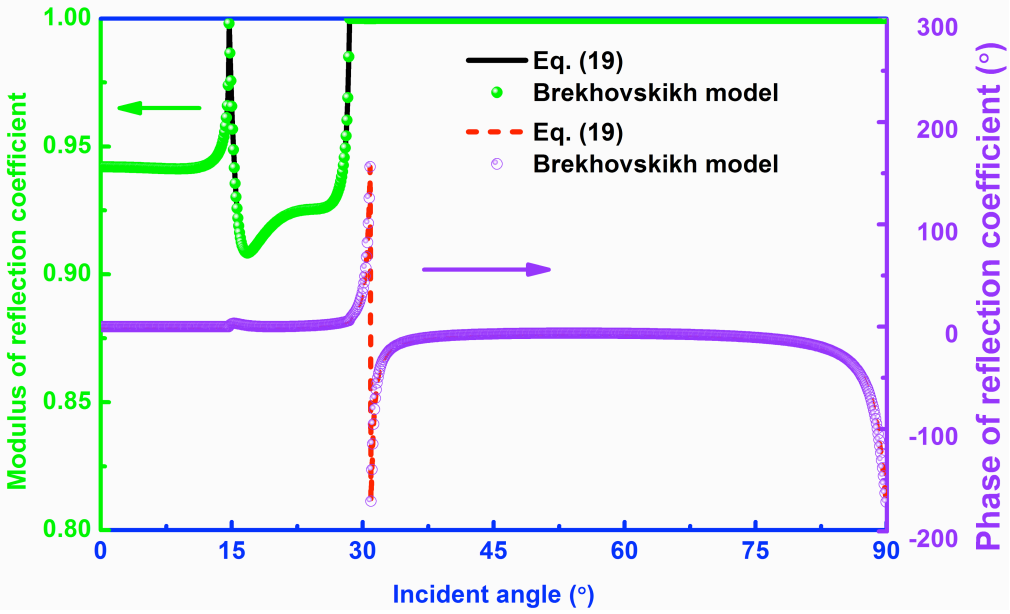

FIG. 5. Comparison of reflection coefficient calculated with Eq. (19) and Eq. (23) of Brekhovskikh model[38] at 18.5 MHz.

B. *V(z)* curves of coatings on substrate

Fig. 6 is a comparison between experimental data and modeling on an Inconel 600 bulk material at 10 MHz. And the reflection coefficient was calculated based on Eq. (19). Good agreement is observed between the modeling and experimental *V(z)* curves. The deviation probably due to the input properties of the coatings and substrate material used in the modeling are different from the actual properties of the material. This disagreement can be reduced or eliminated by an optimization procedure in which the properties of the coating and substrate materials can be adapted and will be discussed in the following Sec. IV.C.

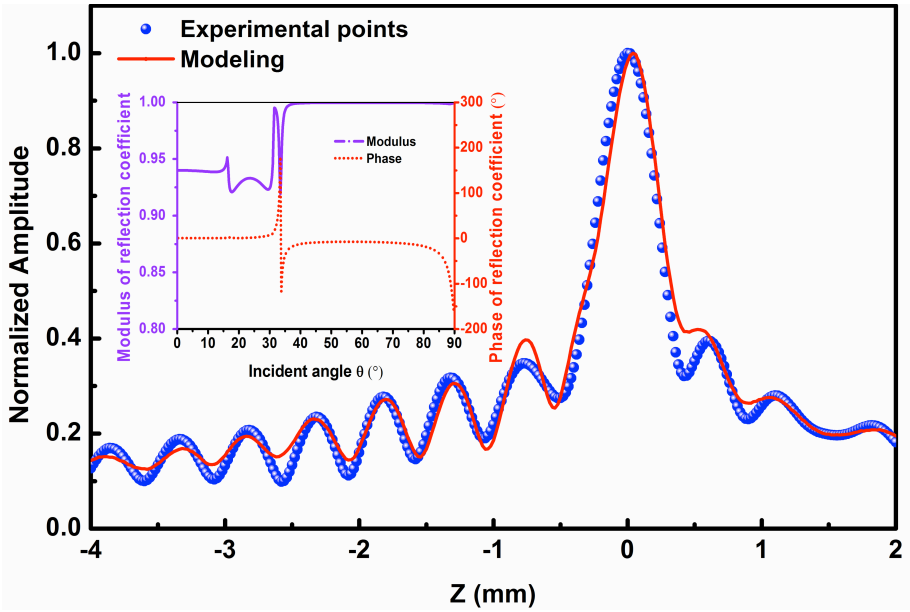

FIG. 6. *V(z)* modeling and experimental comparison of the Hastelloy C22 coating on the 304-type austenitic stainless steel at 10 MHz. The coating thickness is 125 μm.

In order to study the coating thickness sensitivity, *V(z)* curves of different coating thickness are presented in Fig. 7. The curves of the bulk Hastelloy and the 304 stainless steel as substrates (without coatings) are also presented and compared. It is observed that the *V(z)* curved of the coated material varied between the boundary formed by the *V(z)* curved of the bulk 304 stainless steel ($V_s(z)$) and bulk Hastelloy C22 coating ($V_c(z)$) as substrates. This is because that for coating of very small thickness the properties of the substrate dominate the measured acoustic signals and the measured *V(z)* curve behaves like the one of the bulk substrate, i.e., $V_s(z)$. As the thickness of the coating increase, the properties of the coating begin to dominate the reflected acoustic signals and the *V(z)* curve is similar to the one of the bulk coating material, i.e., $V_c(z)$. It is also shown that the *V(z)* curve of the coating thickness of 170 μm is the most discriminative compared to the curves of both $V_s(z)$ *and* $V_c(z)$ at 6 MHz, with a $f \times d$ = 1 MHz·mm. In other words, 6 MHz it is the most suitable frequency to measure a coating of thickness 170 μm. For coatings of other thicknesses, other frequencies should be applied, keeping $f \times d$ in the 0.5 to 3 MHz·mm range. Outside this range, the measured curves becomes too close to $V_s(z)$ or $V_c(z)$, and the coating thickness measurement is less accurate.

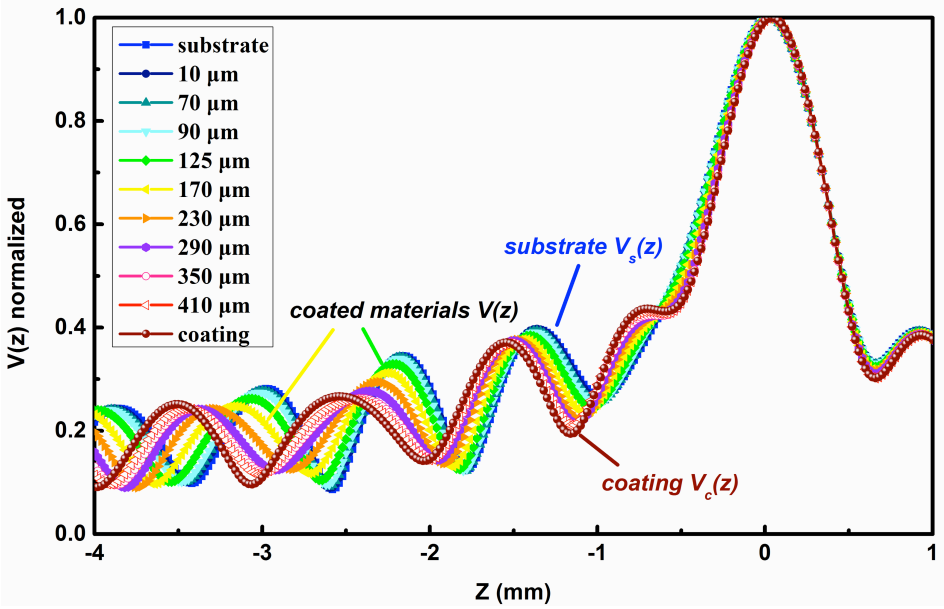

FIG. 7. ***V(z)*** **curves of coated material with different coating thickness as well as curves of the 304-type austenitic stainless steel (*$V_s(z)$*) and the Hastelloy C22 coating (*$V_c(z)$*) materials as substrates, the applied frequency is 6 MHz.**

Fig. 8(a) are *V(z)* curves of the coated material at 6 MHz with a Young's modulus of the coating varying from 160 to 300 GPa. It shows how *V(z)* curves are also sensitive to the Young's modulus of the coating, which indicates *V(z)* measurement could be a good way to evaluate the elastic properties of the coating, if the coating thickness is otherwise well controlled. Fig. 8(b) are *V(z)* curves of the coated material at 6 MHz with a Poisson ratio of the coating varying from 0.1 to 0.46. It shows that *V(z)* curves are almost insensitive to the variation of Poisson ratio. In addition, both Fig. 7 and Fig. 8 show that that *V(z)* curves show little difference between materials of different coating thickness in the range of $z>0$. This phenomena has its roots in the effect of geometric-related waves at positive defocus ($z>0$) and thus in this range the *V(z)* curves are dominated by the geometric properties of the transducer and the coupling fluid.[16] Therefore, the focus will thereafter be put on the negative defocus ($z<0$), i.e., the left parts of the *V(z)* curves, for the analysis of the properties of the materials under evaluation.

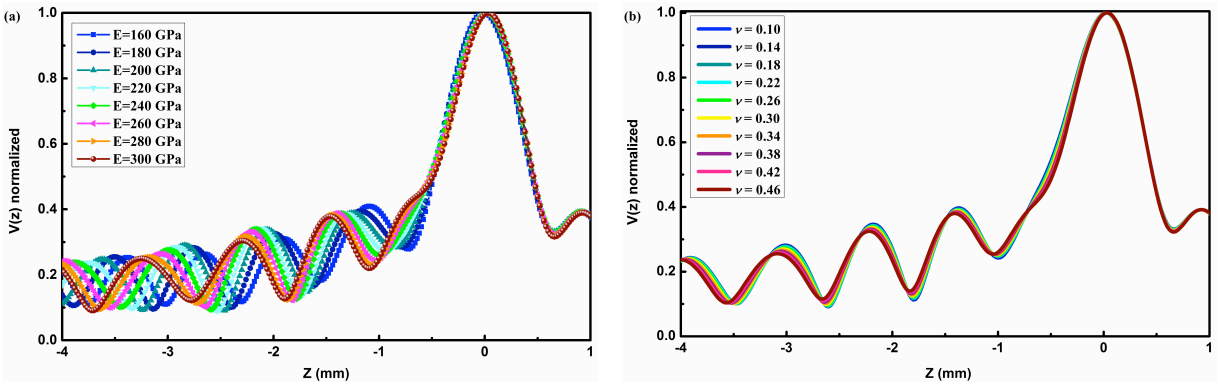

(a) (b)

FIG. 8. ***V(z)*** **curves of the Hastelloy C22 coating on the 304-type austenitic stainless steel at 6 MHz with a coating thickness of 100 μm, (a) with coating Yong's modulus varying from 160 to 300 GPa and (b) Poisson ratio varying from 0.1 to 0.46.**

C. Data inversion and coating thickness measurement

For layered system on substrate, a 22-type Hastelloy coating thermally sprayed on a substrate of 304-type austenitic stainless steel is investigated. The surface of the substrate has been shot-peened to increase the adhesion of the coating. Various coating thickness ranging from 100 to 400 µm have been tested. Every sample was slightly polished in order to eliminate the effect of the roughness of the coating.

The measured *V(z)* curves are functions of the parameters of the transducer (focal length, aperture angle), the properties of the material such as elastic tensor elements C_{ijkl}, density ρ, coating thickness d, and the applied frequency f as well as the properties of the coupling fluid. The bounding condition of the coating and the substrate also affect the measured *V(z)* curves, but in this article perfect interfacial conditions were considered. For a fixed transducer and coupling fluid, the *V(z)* curves vary as the coating properties and thickness change. The objective of the data inversion is to determine features of the assumed isotropic thermal sprayed 22-type Hastelloy coatings, e.g., Young's modulus E, Poisson's ratio v, and the coating thickness d.

Fig. 9 shows the experimental and the optimized *V(z)* curves of coated materials with different coating thickness at 6 MHz. These measurements were done on one specimen, for which the coating thicknesses was reduced step by step by polishing after each *V(z)* measurement. Again, one observe that the *V(z)* curves are sensitive to the coating thickness, but trends versus coating thickness are different compared to Fig. 7. This can be explained by variation of coating properties along the depth of the coatings, i.e., the properties of the coatings are functions of coating depth. An reverse analysis (or optimization process) was carried out to fit the *V(z)* curves and to obtain the coating parameters such as coating thickness d, the average (or mean) value of Young's modulus E within the "remaining thickness of the coating", density ρ and Poisson ratio v. Trial values were set into the *V(z)* model and a hybrid minimization method using genetic algorithm coupled with a constrained minimum search function was used to find a set of values of the unknowns that minimizes the deviation between calculated and measured velocities. The deviation function to be minimized is defined as:

$$E_R = \frac{1}{N}\sum_{n=1}^{N}\left[\left(V^{Measured}(z_n) - V^{Calculated}(z_n)\right)^2\right], \tag{24}$$

where N is the number of measured points in z direction.

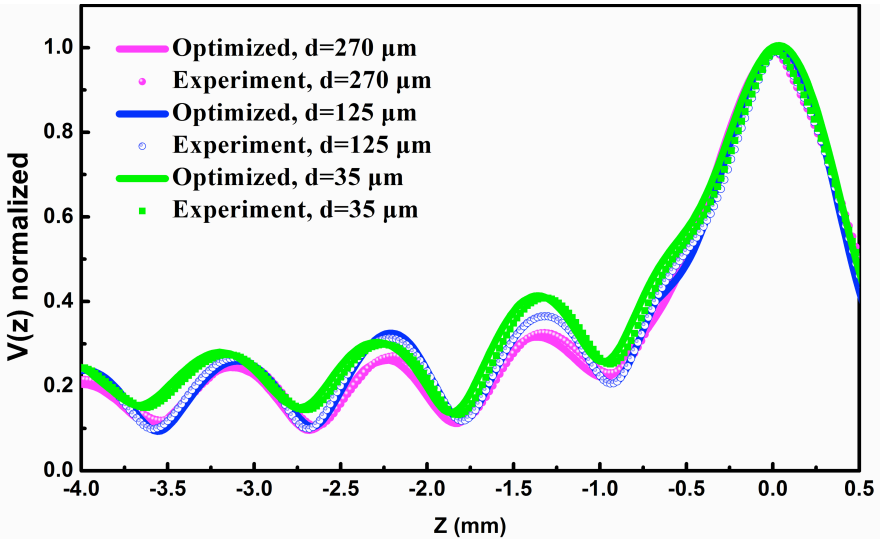

FIG. 9. Experimental and optimized *V(z)* curves of coated materials with different coating thickness at 6 MHz.

During the data inversion process the Poisson ratio and the density are assume to be constant since *V(z)* curve is not sensitive to Poisson ratio as illustrated in Sec. IV.B and the *V(z)* curves are measured on one sample. To our knowledge, according to the conditions of the thermal spraying process, no variation of density is expected within the coating. By this minimization process, the coating thickness and average Young's modulus $\langle E \rangle$ are obtained and the results are plotted in Fig. 10. To your opinion, these results are unique in the sense that no other combination of coating thickness and Young's modulus fits the experimental results. In Fig. 10, an excellent agreement is observed between the coating thickness estimated by reverse analysis of *V(z)* curve and actual coating thickness measured using a micrometer caliper. As the estimated thickness is 100% correlated to the actual thickness, we do not fear any compensation effects between the variations of thickness and average Young's modulus, what indicates that *V(z)* measurement is a powerful tool to evaluate the elastic properties of the coatings.

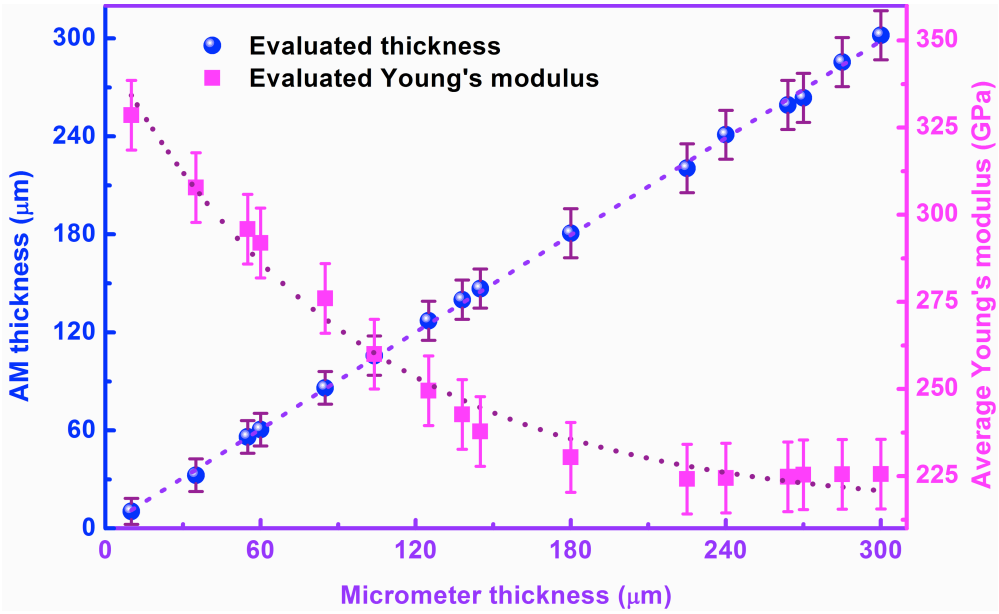

FIG. 10. Coating thicknesses and Young's modulus of 22-type Hastelloy coatings on a substrate of 304-type austenitic stainless steel evaluated by *V(z)* data reversion analysis.

D. Coating with functionally graded properties

Previous work has already shown that *V(z)* measurement can be used to measure the elastic constants of thin films.[9-10,40] But for thick thermal sprayed coating on a substrate, the adaptability of acoustic microscopy is still less studied not only because of the numerical instability[11,20,25,27] during the reverse analysis of *V(z)* curves but also due to the fact that it lacks a powerful numerical tool to deal with the coating of which the properties change along the depth of the thickness. To solve the numerical instability problem, we propose to apply a hybrid method which combines the Stroh formalism and the Recursive Stiffness Matrix method[27] as described in Sec. II.C and IV.B. For the latter, thick layer with varying properties can either be dealt with a multilayered model by dividing it into several homogeneous thin layers or by treating it as a functionally graded material (FGM). These sub-divided homogeneous multilayers can be an asymptotic solution to approximate the real material properties, and the more number of sub-divided multilayers is divided the more precise the approximation will be. The number of layers could be properly chosen in order to obtain a compromise between the approximation precision

and the numerical efficiency. Nevertheless, this multilayer method can be an effective solution compared to an exact functionally graded description method.[36] In this paper, we aim at evaluating the variation of the elastic property in the coating, *ab initio* or as a result of degradation. Since FGM properties are often described by exponential functions.[28,36] we also use the following model:

$$E(z) = E(0) + (E(H) - E(0))\frac{e^{\lambda z/H} - 1}{e^{\lambda} - 1}, \tag{25}$$

where *E(0)* and *E(H)* are the Young's modulus of the upper and lower surface of the coating, respectively, and *H* is the thickness of the coating.

Fig. 11 are measured and calculated *V(z)* curves of a functionally graded coating on substrate with different exponential index λ. Only positive values of λ are considered, because the behavior of <*E(z)*> shown in Fig. 10 indicates that the only possibility for the proposed *E(z)* expression Eq. (25) is to have a positive value of λ. A *V(z)* optimization process was performed to obtain the exponential index of the previously described specimen, which is found to be a functionally graded material along the depth of the coating. The value of the exponential rate that offers the best fit between the measured and modeled values of $\langle E(h)\rangle$ is λ = 5.23. Using this exponential rate in Eq. (25) provides the optimized Young's modulus profile shown in Fig. 12 by the curve with triangle markers.

In order to validate the above evaluated graded Young's modulus profile, further *V(z)* measurements were accomplished by polishing the original 300 μm-thick coating 15 times after each measurement. By doing so, 15 values of average Young's modulus $\langle E(h)\rangle$ over different thicknesses have been determined by the inversion of the corresponding 15 *V(z)* curves under the assumption of homogeneous coating by applying a one-layer on substrate model described in Sec. IV.C. Then, for a *V(z)* curve with a coating thickness of *h*, the profile *E(z)* can be derived from the average Young's modulus $\langle E(h)\rangle$ according to:

$$\langle E(h)\rangle = \frac{1}{h}\int_0^h E(z)dz \tag{26}$$

The first option we chose to retrieve *E(h)* without any *a priori* was to conduct a back-sweep iteration process in order to evaluate the *E(z)* in the coating. First the 15 evaluated average Young's modulus $\langle E(h)\rangle$ as a function of coating thickness *h* were fitted using an exponential curve, then *E(z)* was calculated by a back sweep iteration as:

$$E(h_{i+1}) = \frac{\langle E(h_{i+1})\rangle \times h_{i+1} - \langle E(h_i)\rangle \times h_i}{h_{i+1} - h_i} \tag{27}$$

where $\langle E(h_{i+1})\rangle$ is the average Young's modulus of a coating thickness h_{i+1}, $\langle E(h_i)\rangle$ is that of a coating thickness h_i, and $E(h_{i+1})$ is the Young's modulus at $z=h_{i+1}$.

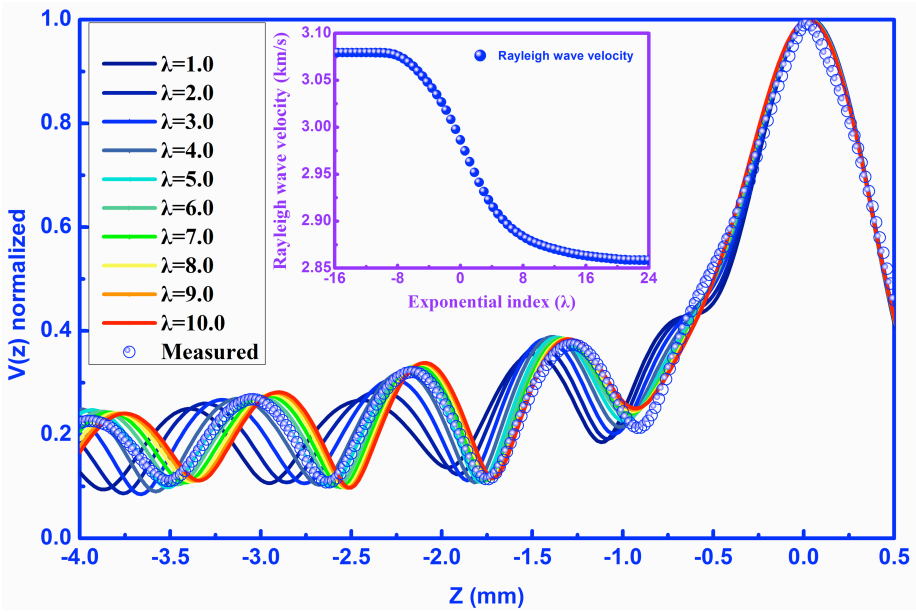

FIG. 11. ***V(z)*** **curves of measured and calculated functionally graded coating on substrate as a function of exponential index** λ**. Inset shows the Rayleigh velocity changes versus the exponential index of the FGM.**

The smaller the (h_{i+1}- h_i) step the more accurate is the approximation of *E(z)*. Hence, the above described procedure was implemented on the $\langle E(h)\rangle$ data interpolated with fine steps, which give the *E(h)* curves with square markers in Fig. 12.

Second, *E(h)* is derived from the measured $\langle E(h)\rangle$ according to the its previously mentioned supposed exponential behavior by substituting Eq. (25) into Eq. (26) and after simple calculation we obtain:

$$\langle E(h)\rangle = E(0) - \frac{\Delta E}{e^{\lambda}-1} + \frac{H}{h}\frac{\Delta E}{\lambda(e^{\lambda}-1)}(e^{\frac{\lambda}{H}h}-1) \tag{28}$$

where h is the thickness of the coating after each etching step; H is 300 μm (the total thickness of the original coating) and $\Delta E=E(H)-E(0)$. The Young's modulus at the bottom of the coating *E(0)* and can be reasonably approximated by the value of $\langle E(h)\rangle$ after the 15^{th} etching step, since the remaining coating thickness is about 20 μm. One can see that there are two remaining parameters to be determined in Eq. (28): λ and ΔE. A data reversion process was conducted applying Eq. (28) in a MatLab curve-fitting program using the measured 15 pairs of $\langle E(h)\rangle$ and h values. The two obtained parameters were λ=5.28 and ΔE=140GPa, which were used in the computation of the *E(h)* profile shown in Fig. 12 by the curve with diamond markers.

Fig. 12 thus enables us to compare the evaluated Young's modulus profile *E(z)* obtained by the optimization of the *V(z)* measured on the raw sample with those obtained by the <*E(h)*> data inversion with or without analytical model. It shows that the proposed exponential Young's modulus model accurately described its actual behavior, since it was validated through destructive measurements.

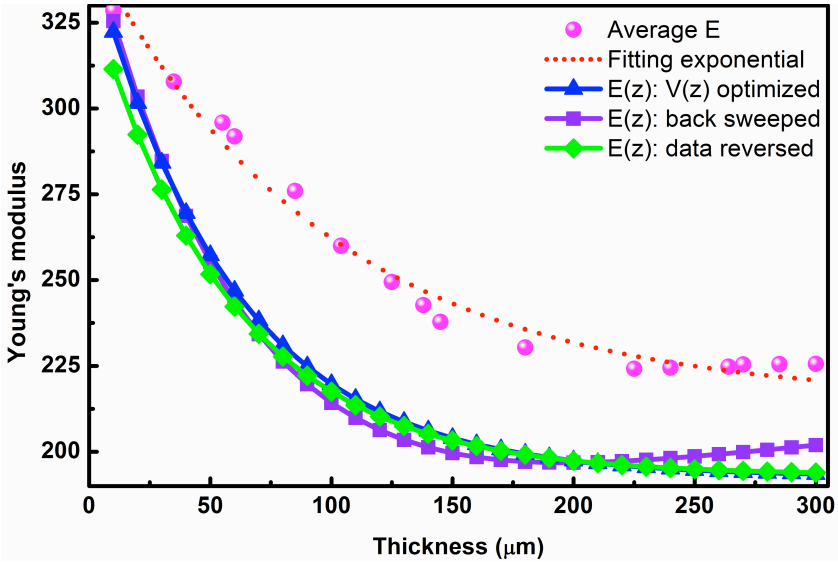

FIG. 12. Comparison of the evaluated Young's modulus gradation *E(z)* by *V(z)* optimization (triangle), back-sweep (square), and data reversion (diamond) methods. The red circled point is the measured average Young's modulus of different coating thickness by etching the coating gradually.

V. CONCLUSION

A model of line-focus microscopy has been derived by angular spectrum approach. Using this model, we studied *V(z)* curves of a thermal sprayed coating on substrate in order to evaluated its elastic properties.

The reflection coefficient for multilayered coatings on a substrate, with fluid loading of the coating's surface, is an integral part of the *V*(*z*) measurement model for a line-focus acoustic microscope. We used a model of multilayered coatings with graded properties on substrate to calculate the acoustic reflection coefficient of our samples. The knowledge of the reflection coefficient is mandatory to investigate SAW propagation in thermal sprayed coatings with different thicknesses.

V(z) curves for different coating thicknesses have been measured and compared with curves based on the established model. Treating 22-type Hastelloy coatings, deposited on a 304 steel substrate, as functionally graded materials (FGM), we evaluated the coating thickness and the Young's modulus gradation independently.

We validated the evolution of the elasticity with depth within the thick coating by means of an iterative, destructive, test. The observed agreement between the results from the FGM model and the multilayered model suggests that we can measure the desired gradient in a completely non-destructive way, which was our initial goal.

ACKNOWLEDGMENTS

The authors are grateful to Dr. Tetsuya Uchimoto (IFS, Tohoku University, Japan) for providing the samples. Xiaodong Deng also acknowledges support from China Scholarship Council (CSC). This work was partly performed within the framework of the Labex CeLyA of Universitée de Lyon, operated by the French National Research Agency (ANR-10-LABX-0060/ ANR-11-IDEX-0007).

References

[1]C. F. Quate, A. Atalar, and H. K. Wickramasinghe, "Acoustic microscopy with mechanical scanning-a review," Proc. IEEE **67**, 1092 (1979).

[2]R. A. Lemons and C. F. Quate, "A scanning acoustic microscope," in *IEEE Ultrasonics Symposium proceedings* (1973), p. 18.

[3]A. Briggs, Acoustic Microscopy (Clarendon, Oxford, 1992).

[4]G. Bourse, W. J. Xu, A. Mouftiez, L. Vandevoorde, and M. Ourak, "Interfacial adhesion characterization of plasma coatings by *V(z)* inversion technique and comparison to interfacial indentation," NDT&E Int. **45**, 22 (2012).

[5]R. D. Weglein, "A model for predicting acoustic material signatures," Appl. Phys. Lett. **34**, 179 (1979).

[6]A. Atalar, "An angular-spectrum approach to contrast in reflection acoustic microscopy," J. Appl. Phys. **49**, 5130 (1978).

[7]Z. L. Li, J. D. Achenbach, and J. O. Kim, "Effect of surface discontinuities on *V(z)* and *V(z,x)* for the line-focus acoustic microscope," Wave Motion **14**, 187 (1991).

[8]K. K. Liang, S. D. Bennett, B. T. Khuri-Yakub, and G. S. Kino, "Precise Phase Measurements with the acoustic Microscope," IEEE Trans. Sonics Ultrason. **32**, 266 (1985).

[9]W. Li and J. D. Achenbach, "Measuring thin-film elastic constants by line-focus acoustic microscopy," in *IEEE Ultrasonics Symposium proceedings* (1995), p. 883.

[10]Z. Q. Guo, J. D. Achenbach, A. Madan, K. Martin, and M. E. Graham, "Modeling and acoustic microscopy measurements for evaluation of the adhesion between a film and a substrate," Thin Solid Films **394**, 189 (2001).

[11]Y. C. Lee, J. O. Kim and J. D. Achenbach, "*V(z)* curves of layered anisotropic materials for the line-focus acoustic microscope," J. Acoust. Soc. Am. **94**, 923 (1993).

[12]H. L. Bertoni and M. G. Somekh, "Ray-Optical Analysis of Spherical Focusing Transducers for Acoustic Microscopy," in *IEEE Ultrasonics Symposium proceedings* (1985**)**, p. 715.

[13]M. G. Somekh, H. L. Bertoni, G. A. Briggs, and N. J. Burton, "A two dimensional imaging theory of surface discontinuities with the scanning acoustic microscope," Proc. R. Soc. **401**, 29 (1985).

[14]D. A. Rebinsky and J. G. Harris, "An asymptotic calculation of the acoustic signature of a cracked surface for the line focus scanning acoustic microscope," Proc. R. Soc. **436**, 251 (1992).

[15]D. Chizhik and D. A. Davids, "Application of a diffraction-corrected ray theory to the slot lens in acoustic microscopy," J. Acoust. Soc. Am. **92**, 3291 (1992).

[16]J. Zhang, P. Guy, J. C. Baboux, and Y. Yajet, "Theoretical and experimental response for large-aperture broadband spherical transducer probing a liquid-solid boundary," J. Appl. Phys. **68**, 2825 (1999).

[17]G. R. Liu, J. D. Achenbach, J. O. Jim, and Z. I. Li, "A combined finite element method/boundary element method technique for *V(z)* curves of anisotropic-layer/substrate configurations," J. Acoust. Soc. Am. **92**, 2734 (1992).

[18]A. H. Fahmy and E. L. Adler, "Propagation of acoustic surface waves in multilayers: A matrix description," Appl. Phys. Lett. **20**, 495 (1973).

[19]E. L. Adler, "Matrix method applied to Acoustic waves in multilayers," IEEE Trans. Ultrason. Ferroelectr. Freq. Control **37**, 485 (1990).

[20]R. Leiderman, A. M. Braga, and P. E. Barbone, "Scattering of ultrasonic waves by defective adhesion interfaces in submerged laminated plates," J. Acoust. Soc. Am. **118**, 2154 (2005).

[21]B. Mandal, "Reflection and transmission properties of elastic waves on a plane interface for general anisotropic media," J. Acoustic. Soc. Am. **90**, 1106 (1991).
[22]E. L. Adler, "SAW and pseudo-SAW properties using matrix methods," IEEE Trans. Ultrason. Ferroelectr. Freq. Control **41**, 876 (1994).
[23]P. M. Smith, "Dyadic Green's functions for multi-layer SAW substrates," IEEE Trans. Ultrason. Ferroelectr. Freq. Control **48**, 171 (2001).
[24]M. Castaings and B. Hosten, "Delta operator technique to improve the Thomson–Haskell - method stability for propagation in multilayered anisotropic absorbing plates," J. Acoust. Soc. Am. **95**, 1931 (1994).
[25]T. Pastureaud, V. Laude, and S. Ballandras, "Stable scattering-matrix method for surface acoustic waves in piezoelectric multilayers," Appl. Phys. Lett. **80**, 2544 (2002).
[26]A. Reinhardt, T. Pastureaud, S. Ballandras, and V. Laude, "Scattering matrix method for modeling acoustic waves in piezoelectric, fluid, and metallic multilayers," J. Appl. Phys. **94**, 6923 (2003).
[27]S. I. Rokhlin and L. Wang, "Stable recursive algorithm for elastic wave propagation in layered anisotropic media: Stiffness matrix method," J. Acoust. Soc. Am. **112**, 822 (2002).
[28]L. Wang and S. I. Rokhlin, "Recursive asymptotic stiffness matrix method for analysis of surface acoustic wave devices on layered piezoelectric media," Appl. Phys. Lett. **81**, 4049 (2002).
[29]C. Baron, "Le développement en série de Peano du matricant pour l'étude de la propagation des ondes élastiques en milieux à propriétés continûment variables", Ph.D. dissertation (Université de Bordeaux, Bordeaux , 2005).
[30]J. D. Achenbach, "Modeling for quantitative non-destructive evaluation," Ultrasonics **40**, 1 (2002).
[31]A. N. Stroh, "Steady state problems in anisotropic elasticity," J. Math. Phys. **41**, 71 (1962).
[32]A. K. Mal, "Wave propagation in layered composite laminates under periodic surface loads," Wave Motion **9**, 231 (1988).
[33]J. R. Barber and T. C. T. Ting, "Three-dimensional solutions for general anisotropy," J. Mech. Phys. Solids. **55**, 1993 (2007).
[34]T. C. T. Ting and D. M. Barnett, "Classifications of surface waves in anisotropic elastic materials," Wave Motion **26**, 207 (1997).
[35]K. Tanuma, "Stroh Formalism and Rayleigh Waves," J. Elasticity **89**, 5 (2007).
[36]L. Wang and S. I. Rokhlin. "Recursive geometric integrators for wave propagation in a functionally graded multilayered elastic medium," J. Mech. Phys. Solids. **52**, 2473 (2004).
[37]A. H. Nayfeh, Wave Propagation in Layered Anisotropic Media (Elsevier, Amsterdam, 1995).
[38]Z. Q. Guo, J. D. Achenbach, A. Madan, K. Martin, and M. E. Graham, "Integration of modeling and acoustic microscopy measurements for thin films," J. Acoust. Soc. Am. **107**, 2462 (2000).
[39]L. M. Brekhovskikh, Waves in Layered Media (Academic, New York, 1980), Chap. 1, p. 44.
[40]A. Tourlog, W. Li, and J. D. Achenbach, "Line-focus acoustic microscopy measurements of elastic constants for materials with high acoustic velocities," Appl. Phys. Lett. **69**, 3680 (1996).